PAN
POLISH ACADEMY OF SCIENCES

Opto-Electronics Review

journal homepage: http://journals.pan.pl/opelre

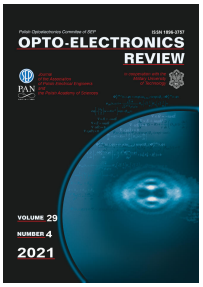

Formula for temperature distribution in multi-layer optical fibres for high-power fibre lasers

M. Grábner*, P. Peterka, P. Honzátko

Department of Fiber Lasers and Nonlinear Optics, Institute of Photonics and Electronics, Czech Academy of Sciences, 1014/57 Chaberská St., 18251 Praha 8, Czech Republic

Article info

Article history:
Received 10 Sep. 2021
Received in revised form 22 Oct. 2021
Accepted 23 Oct. 2021
Available online 12 Nov. 2021

Keywords:
High-power fibre lasers, active optical fibres, temperature distribution, heat transfer.

Abstract

High power fibre lasers need to be cooled efficiently to avoid their thermal damage. Temperature distribution in fibre should be estimated during the fibre laser design process. The steady-state heat equation in a cylindrical geometry is solved to derive a practical formula for temperature radial distribution in multi-layered optical fibres with arbitrary number of the layers. The heat source is located in one or more cylindrical domains. The validity of the analytical formula is tested by comparison with static heat transfer simulations of typical application examples including octagonal double clad fibre, air-clad fibre, fibre with nonuniform, microstructured core. The accuracy sufficient for practical use is reported even for cases with not exactly cylindrical domains.

1. Introduction

Thermal management of high-power fibre lasers [1] is an indispensable part of their design. As the pump power is absorbed in the active area of the fibre-doped core, the part of absorbed power is transformed to heat that increases the fibre temperature. To avoid thermal damage of the fibre and its coating, heat should be efficiently transferred away by a medium surrounding the fibre. The cooling efficiency can be assessed based on the estimation of temperature distribution in the fibre cross-section which, in turn, depends on the intensity of the heat source, i.e., the power absorbed, and on the thermal parameters of the fibre cross-section structure.

Several works studied temperature distribution in fibre lasers from different perspectives. A time domain heat transfer analysis of doped fibres was presented [2]. A formula for the temperature distribution in a two-layer fibre was derived from a steady-state heat equation [3]. The thermo-optical behaviour of air-clad photonic crystal fibre lasers was investigated, as well [4]. Thermal influences on kilowatt Yb-doped double-clad fibre lasers were studied numerically [5]. An analytical approach for the thermal design of high-power lasers based on one dimensional heat equation was also presented [6]. Thermal effects in high-power CW fibre lasers were studied by solving the radial heat equation [7]. Transient heat conduction and thermal effects in a pulse end-pumped fibre laser were analytically solved [8].

Temperature distribution in a double-clad fibre as a function of the heat load was obtained using a finite element method [9]. Heat transfer equation was analytically solved for the case of a high-power fibre laser with a double cladding [10]. Relation for the temperature distribution in a three-layer cylindrical structure of a double-clad fibre was given [11] and an efficient heat transfer technique was discussed [12]. Considering [3] and [11], temperature dependent effects in Tm-doped fibres lasers were analysed [13]. An analytical temperature model based on a thermal conduction equation was reported for double-clad Yb-doped fibre lasers [14]. Thermal characteristics of Tm-doped fibre lasers in double-clad and triple-clad arrangements were also studied based on the analytical model of the radial temperature distribution [15]. An efficient cooling of fibre lasers by means of a metal cladding was presented, as well [16]. A thermal distribution with different heat sources and an analytical solution of the heat transfer equation in double-clad fibres were investigated [17]. An analytical thermal resistance model

*Corresponding author at: grabner@ufe.cz

https://doi.org/10.24425/opelre.2021.139482
1896-3757/ Association of Polish Electrical Engineers (SEP) and Polish Academic of Sciences (PAS). Published by PAS

was proposed and applied to calculate heat dissipation in an Yb-doped double-clad fibre [18]. Recently, temperature distribution inside a double-cladding optical fibre laser was examined [19].

In the works cited above, the number of the considered cylindrical layers is limited or there is no explicit formula presented for cases with a higher number of layers. However, in some applications, the number of cylindrical layers forming the fibre and its surrounding is higher than two or three that has been usually assumed in theoretical approaches, so far. Numerical simulation is possible in those cases, but it is not practical for the structure design optimization, or it is not even needed for the initial estimation of the temperature distribution.

In this paper, a simple analytical formula is derived for temperature distribution in cylindrical optical fibre structures with *arbitrary* number of layers. The validity of the formula is tested by comparison with finite element computations of typical application examples.

2. Analytical model

The analytical formula for the radial distribution of temperature was given in Ref. 3 for a two-region static heat transfer problem in cylindrical geometry. The basic form of the model that was used in further works is as follows:

$$T_1(r) = T_0 - \frac{Q_1 r^2}{4k_1}, \tag{1}$$

$$T_2(r) = T_0 - \frac{Q_1 a_1^2}{4k_1}\left(1 + 2\ln\frac{r}{a_1}\right), \tag{2}$$

$$T_0 = T_b + \frac{Q_1 a_1^2}{4k_1}\left(1 + 2\ln\frac{a_2}{a_1}\right), \tag{3}$$

where the notation of quantities involved is described below. The generalization of the problem for the case of N cylindrical layers (see Fig. 1) considered here is defined as:

$$\nabla^2 T_n = -\frac{Q_n}{k_n} \quad \text{for layers } n = 1, \ldots, N \tag{4}$$

with interface boundary conditions:

$$T_N(a_N) = T_b \tag{5}$$

$$T_n(a_n) = T_{n+1}(a_n) \tag{6}$$

$$\frac{dT_1(0)}{dr} = 0 \tag{7}$$

$$k_n \frac{dT_n(a_n)}{dr} = k_{n+1}\frac{dT_{n+1}(a_n)}{dr} \tag{8}$$

for $1 \le n < N$ where r [m] is a distance from the centre, $T_n(r)$ [°C] is the temperature radial profile, Q_n [W/m^3] is the power density of a heat source, a_n is the outer radius of the n-th layer, k_n [Wm^{-1}K^{-1}] is the thermal conductivity, T_b is the boundary (background) temperature. Here, the subscript n means that the variable is evaluated in the n-th layer counted from the centre. The heat power density Q_n

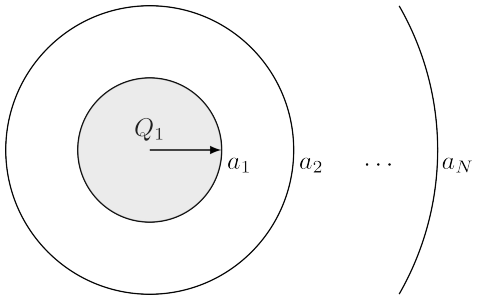

Fig. 1. The geometry of the static heat transfer problem in N cylindrical layers with the heat source Q_1 in the innermost domain.

is assumed to be constant within the n-th layer and is zero in layers without the heat source. Generally, if the line heat power density (or heat load) Q_l [W/m] is given, the volume density is obtained as $Q = Q_l/A$ where A is the domain cross-section area of the heat source.

Assuming that all relevant quantities of the problem are isotropic and independent of the longitudinal coordinate z, the left-hand side of Eq. (4) is $\nabla^2 T = \frac{d^2T}{dr^2} + (1/r)\frac{dT}{dr}$. A homogeneous solution of Eq. (4) is obtained by a separation of variables giving $\frac{dT_n}{dr} = C_n/r$ where C_n are constants and $1 \le n < N$. An inhomogeneous solution of Eq. (4) is obtained by variation of constants as $T_n(r) = -\frac{Q_n}{4k_n}r^2 + C_n \ln r + T_{0n}$ where C_n and T_{0n} are the constants. From the condition in Eq. (7), it follows $C_1 = 0$. From the conditions in Eq. (8), the relation for C_n in terms of C_{n-1} is determined. Finally, the conditions in Eqs. (5) and (6) are applied consecutively to determine the additive constants T_{0n}. The resulting formula for the radial temperature distribution is:

$$T_n(r) = T_{01} + K_n(r), \quad 1 \le n \le N \tag{9}$$

where:

$$K_1(r) = \frac{\tau_1}{4}r^2 \tag{10}$$

$$K_n(r) = \frac{\tau_n}{4}(r^2 - a_{n-1}^2) + C_n \ln\frac{r}{a_{n-1}} + \sum_{i=1}^{n-1}\frac{\tau_i}{4}(a_i^2 - a_{i-1}^2) + \sum_{i=2}^{n-1} C_i \ln\frac{a_i}{a_{i-1}} \tag{11}$$

for $1 < n \le N$,

with $\tau_n = -Q_n/k_n$ and the constants:

$$T_{01} = T_b - K_N(a_N), \tag{12}$$

$$C_n = \frac{k_{n-1}}{k_n}C_{n-1} + \frac{a_{n-1}^2}{2}\left(\frac{k_{n-1}}{k_n}\tau_{n-1} - \tau_n\right). \tag{13}$$

In Eqs. (11) and (13), the quantities with zero index are assumed to be zero.

The analytical model in Eqs. (9)–(13) can be considered as a straightforward generalization of Eqs. (1)–(3) or of their particular extensions presented in literature, so far.

Nevertheless, it has a great potential for the practical usage, e.g., as a part of fibre laser/amplifier models based on the solution of laser rate equations [20,21], since quite often the higher number of cylindrical domains with different thermal conduction properties are involved in active fibre problems and numerical simulations are computationally too demanding for the purpose. In particular, the outer layers of the fibre, its coating and the surrounding environment can have significant impact on the overall temperature distribution in the cross-section of the fibre structure. This will be also demonstrated in the next section where the validity of the analytical model Eqs. (9)–(13) is checked by means of several application examples.

3. Test problems

3.1. Fibre in circular slot

The first fibre heating test problem is defined as follows. The fibre is modelled as a 5-layer cylinder with the layers 1, 2 composed of silica, the layer 3 of a polymer, the layer 4 of a Sylgard 184 kit, and the layer 5 is made of aluminium. Note that the Sylgard 184 kit is used here only as an example and there are other materials that are more suitable for the applications of high-power fibre lasers due to their higher thermal conductivity. The geometrical and material parameters of a fibre cross-section are summarized in Table 1 where the domain radius a and the thermal conductivity values k are stated. The boundary (or background) temperature is set to $T_b = 22$ °C in all test problems.

Table 1.
Cross-section geometry parameters, radius a and thermal conductivity k.

n	Material/domain	a_n [μm]	k_n [Wm^{-1}K^{-1}]
1	SiO_2 core	12.5	1.38
2	SiO_2 cladding	200	1.38
3	Polymer coating	280	0.18
4	Sylgard 184	400	0.27
5	Aluminium	450	238

Figure 2 compares the analytical solution with the numerical one computed by the finite element method (FEM) in COMSOL with the same geometry. Both solutions are identical, but one should note that the temperature distribution evaluation by an analytical model is faster by orders of magnitude than a FEM simulation. This is advantageous especially when a temperature model serves as part of some sort of feedback mechanism inside the fibre laser model (e.g., temperature dependent absorption and emission spectra) where iterations are needed to find a solution [20,21].

It is instructive to see how the temperature at the critical point on the boundary of cladding and coating depends on the heat load. Figure 3 shows that the temperature increases with the heat load with a slope determined by the cladding radius, provided that all other parameters are fixed. Considering a polymer temperature limit of around 80 °C that should not be exceeded [16], a sufficiently large cladding radius is needed to stand a given heat load with no polymer coating damage.

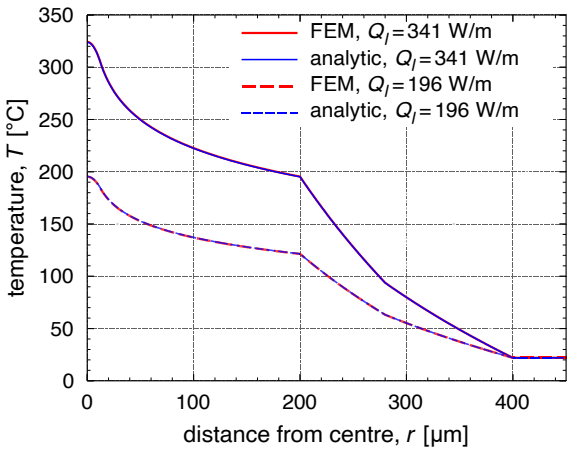

Fig. 2. Radial distribution of the fiber temperature in the circular slot.

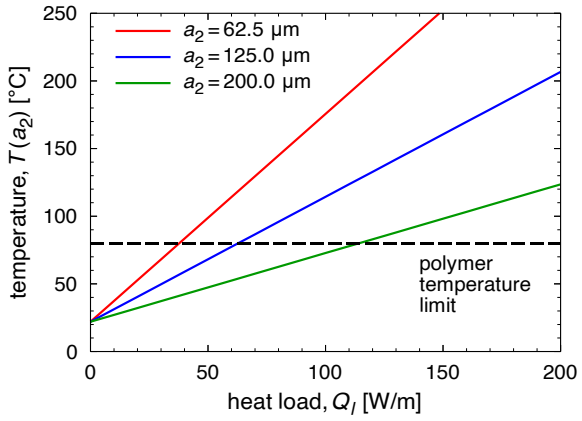

Fig. 3. Temperature at silica/polymer boundary ($r = a_2$) as a function of the heat load for several cladding radii a_2.

Finally, let us briefly comment on the relation between the heat load and the pump power. Both the pump power evolution along the fibre and the corresponding local heat load can be estimated using numerical models of the active fibre [20,21]. The heat load can be also roughly estimated considering the pump absorption A_p [dB/m] that is *constant* along the fibre (see e.g., [22] for a more realistic model of the pump absorption) and assuming the constant power conversion efficiency η [–]. Then the resulting heat load Q_l [W/m] along the fibre as a function of the length coordinate z [m] can be expressed as:

$$Q_l(z) = (1-\eta)P_p(0)a_p \exp(-a_p z), \qquad (14)$$

where $a_p = (A_p/10)\ln 10$ and $P_p(0)$ [W] is the input pump power. For $P_p(0) = 1200$ W, $A_p = 3$ dB/m and $\eta = 0.59$, it gives $Q_l(0) = 340$ W/m at the beginning of the fibre.

3.2. Octagonal cladding fibre

As the second example, an octagonal cladding fibre with a flat-to-flat size FtF = 250 μm is selected. Octagonal and other polygonal shapes are typical examples of breaking the circular symmetry of the cross-section of double-clad fibres. Such cross-sections are beneficial for mode scrambling and correspondingly improved pump

absorption [1,22]. Figure 4 shows the cross-section geometry and the spatial distribution of temperature obtained from a numerical simulation. The materials and background temperature are the same as in the previous example but a more realistic scenario with the fibre located inside a *square groove* is analysed.

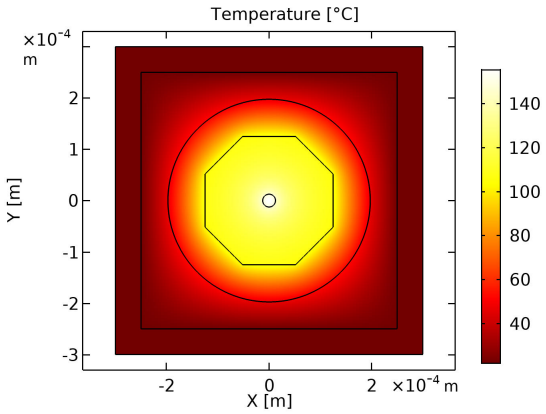

Fig. 4. Spatial distribution of temperature in the octagonal cladding fiber for Q_l = 150 W/m.

Figure 5 compares the analytical model (with 5 layers) with a simulation for two values of a heat power density. Here, the distance from the centre is measured along the x - axis. Analytical model slightly underestimates the temperature in a whole region of distances. When the fibre is in the corner of the square groove so that the polymer layer touches the alumina walls, which is the realistic assumption, the temperature profile becomes non-symmetrical with respect to the fibre centre.

Figure 6 compares the model and simulation in that case. The analytical formula still provides fairly accurate results with the highest error being at the outer regions where the temperature is low.

3.3. *Fibre with nonuniform core*

In the examples analyzed so far, the core is assumed to be uniformly doped resulting in a constant power density of the heat source in the entire core area. There are, however, alternative designs possible. Figure 7 shows the core cross-section of the radius r_c with 7 doped rods in a hexagonal setup.

Shaded circles are the doped areas with the diameter t, the dashed circles denote preform tubes stacked together during a fibre drawing process. Since the area of the doped domain and so of the heat source is smaller than the core area, the temperature is expected to form hot spots in doped rods. The analytical model assuming cylindrical symmetry cannot describe such structure precisely but one can approximate it by an equivalent structure with the doped layer of thickness t_1, see Fig. 7. In order to maintain the same heat source density, the area of this layer has to be the same as the total area of 6 outer rods in the original structure. In our case, it follows that $t_1 = 9t^2/(8r_c)$.

The radial distribution of temperature in the octagonal cladding fibre with 7 doped rods in the core was obtained using FEM (see Fig. 8) and in the equivalent 8-layer structure using the analytical model with the results presented in Fig. 9.

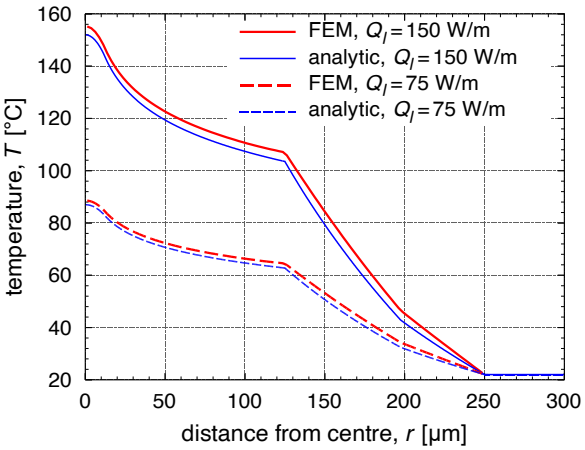

Fig. 5. Radial distribution of temperature in the octagonal cladding fiber.

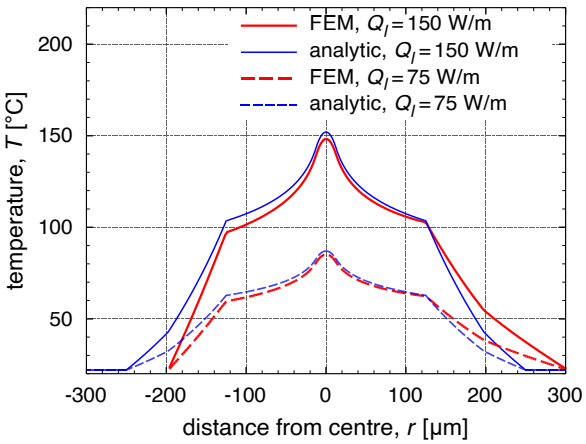

Fig. 6. Radial distribution of temperature in the octagonal cladding fiber located in the corner of the square slot.

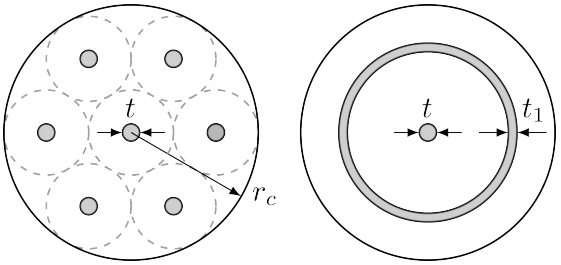

Fig. 7. Scheme of the core cross-section with 7 doped rods (left) and an approximately equivalent structure (right) with a doped layer with the same cross-section area as 6 outer rods.

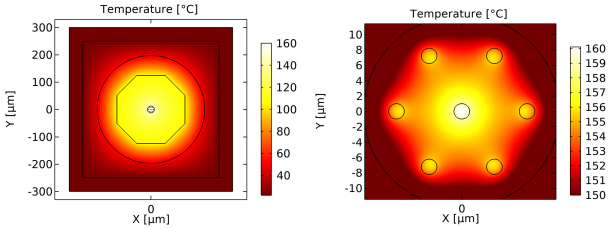

Fig. 8. Spatial distribution of temperature in the octagonal cladding fiber with a core with 7 doped rods. Left: entire cross-section, right: core area.

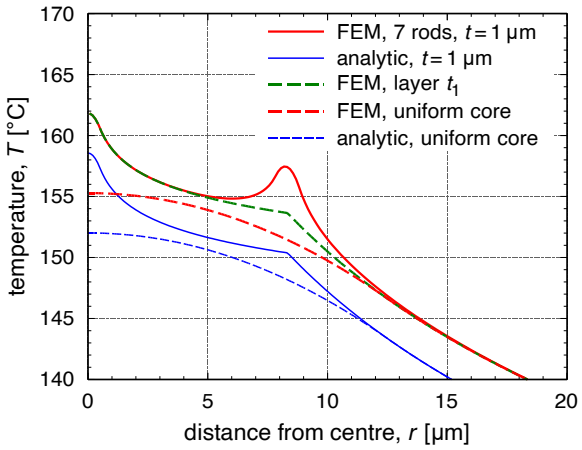

Fig. 9. Radial distribution of temperature in the octagonal cladding fiber. 7 doped rods with the diameter $t = 1$ µm *vs*. the uniformly doped core with the same heat load $Q_l = 150$ W/m.

Compared to the uniformly doped core, the local temperature peaks at the centre and on the outer rod are predicted by FEM simulation. While the local temperature hot spot on the outer rod is not predicted by the model, it is evident that the peak temperature at the central hotspot is predicted very well by the model, the temperature shift being due to the non-circular shape of outermost layers. Apart of this shift, the analytical model gives the same temperature profile as FEM simulation with the same layered structure of the core.

In practice, the micro- or nanostructured core [23,24] can be applied to decrease the average doping concentration in the core to values that would not be available in the case of uniformly doped core due to a lower limit of concentration given by technological restrictions. For example, the rare earth ions concentration higher than 3.5 wt% is necessary for the efficient operation of a high-power thulium fibre laser exploiting so-called two-for-one cross-relaxation optical pumping [25,26].

Figure 10 presents a comparison of the temperature profiles in a uniformly doped core and the core with 7 doped rods in the case of the same concentration and, thus, the same heat density. In the uniform core, the temperature is much higher than in the micro-structured core since the

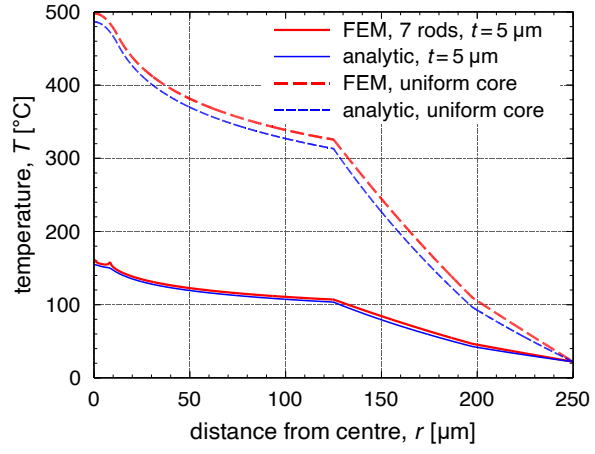

Fig. 10. Radial distribution of temperature in the octagonal cladding fiber. 7 doped rods with $t = 5$ µm *vs*. the uniform core with the same heat density $Q = 1.1 \cdot 10^{12}$ W/m^3.

different values of heat load are related by the ratio of doped areas in both scenarios.

3.4. *Air-clad fibre*

As a final example, an air-clad fibre is analysed with the geometry depicted in Fig. 11, where also the spatial temperature distribution obtained from the FEM simulation is shown. In the simulation of the air-clad fibre, the thermal conductivity of air [27] was defined using the polynomial formula:

$$k_{\mathrm{air}}(T) = \sum_{i=0}^{3} c_i T^i , \tag{15}$$

with coefficients $c_0 = -3.9333 \cdot 10^{-4}$, $c_1 = 1.0184 \cdot 10^{-4}$, $c_2 = -4.8574 \cdot 10^{-8}$, $c_3 = 1.5207 \cdot 10^{-11}$ where the temperature T is expressed in Kelvins. A typical value of the thermal conductivity of air is $k_{\mathrm{air}} = 0.034$ Wm^{-1}K^{-1} for $T = 140$ °C.

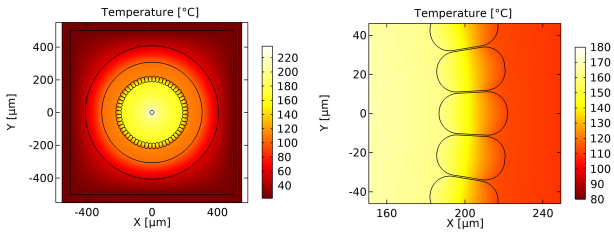

Fig. 11. Spatial distribution of temperature in the air-clad fiber for $Q_l = 200$ W/m. Left: entire cross-section, right: detail of air hole shapes.

However, the layer of air cladding contains also narrow silica bridges that greatly increase the heat transfer away from the fibre centre area compared with the pure air layer case. Therefore, when an analytical model is to be applied in the case of the air-clad fibre, the effective value of the thermal conductivity k_{ef} of the air-clad layer should be used:

$$k_{\mathrm{ef}} = k_{\mathrm{air}} \frac{w_{\mathrm{air}}}{w_{\mathrm{air}} + w_{\mathrm{SiO_2}}} + k_{\mathrm{SiO_2}} \frac{w_{\mathrm{SiO_2}}}{w_{\mathrm{air}} + w_{\mathrm{SiO_2}}} , \tag{16}$$

where in our example $w_{\mathrm{SiO2}} = \alpha \cdot 0.72$ µm ($\alpha = 1.3$) is the *effective* thickness of the silica bridges and $w_{\mathrm{air}} = 20.35$ µm is the respective width of the air domains in the azimuth direction. Note that the effective thickness w_{SiO2} is larger than the smallest bridge thickness since the rounded shape of the air holes should be considered, see Fig. 11 (right). Also, the application of Eq. (16) is of great importance because about 90 °C higher core temperature value is obtained from the model using the simple relationship $k_{\mathrm{ef}} = k_{\mathrm{air}}$. Furthermore, in order to respect Eq. (15) in the analytical model, several iterations are applied where the temperature determined in the centre of the air-clad layer is chosen as the input of Eq. (15) in the next iteration.

Figure 12 compares an analytical solution (with 7 layers) with a numerical one computed by FEM. The solution is fully consistent with the FEM simulation of the air-clad fibre presented in Ref. 28. The analytical solution agrees very well with the numerical one, but it underestimates temperature in layers outside the air-clad

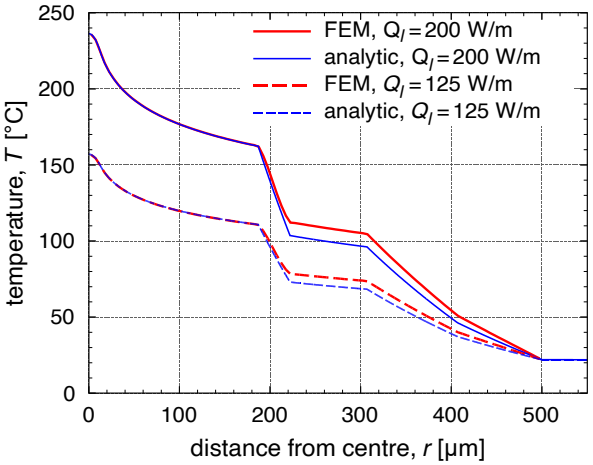

Fig. 12. Radial distribution of temperature in the air-clad fiber.

layer. This could again be attributed to the square shape of the groove.

Finally, the similar methodology presented here for the case of the air-clad fibre can be in principle applied even for other similar fibre structures, e.g., for large-pitch photonic crystal fibres [29,30], provided that the effective thermal conductivity is determined also in the micro-structured part of the fibre.

4. Conclusions

The analytical formula for the radial temperature distribution in multi-layer optical fibres was presented and tested in comparison with the FEM simulation results. A detailed review of the previous works on analytical formulas for the temperature distribution in optical fibres for high-power fibre lasers is provided. Contrary to previous works, devoted to the cases with specific number of layers (typically three), a generalized formula that comprises an arbitrary number of cylindrical layers and a heat source located in arbitrary layers is presented in the paper. The derived formula is practical for a range of optical fibre arrangements; three specific examples known from applications are reported to demonstrate the applicability of the formula. Although the formula was derived for the case of completely cylindrical geometry including a cooling medium, it was demonstrated by the analysis of octagon shape and air-clad fibres that it was fairly accurate even in more realistic scenarios with a fibre inside a square groove. The presented model can be in principle also applied in the case of nonuniform heat sources if they can be approximated by several cylindrical layers with the uniform heat distribution. It is envisaged that the presented formula can serve well not only for a fast estimation of the radial temperature distribution in multi-layer fibres, but it can also be part of more complex temperature-dependent fibre laser models.

Authors' statement

Research concept and designs, P. P. and P. H.; collection and/or assembly of simulation data, M. G.; data analysis and interpretation, M. G.; analytical model development M. G.; writing the article, M. G.; critical revision of the article, P. P. and P. H.; final approval of article, M. G., P. P. and P. H.

Acknowledgements

This research was sponsored by the Czech Science Foundation through the project No. 19-03141S.

References

[1] Zervas, M. N. & Codemard, C. . High power fiber lasers: A review. *IEEE J. Sel. Topics Quantum Electron.* **20**, 219–241 (2014). https://doi.org/10.1109/JSTQE.2014.2321279

[2] Davis, M. K., Digonnet, M. J. F. & Pantell, R. H. Thermal effects in doped fibers. *J. Light. Technol.* **16**, 1013 (1998). https://doi.org/10.1109/50.681458

[3] Brown, D. C. & Hoffman, H. J. Thermal, stress, and thermo-optic effects in high average power double-clad silica fiber lasers. *IEEE J. Quantum Electron.* **37**, 207–217 (2001). https://doi.org/10.1109/3903070

[4] Limpert, J. *et al*. Thermo-optical properties of air-clad photonic crystal fiber lasers in high power operation. *Opt. Express* **11**, 2982–2990 (2003). https://doi.org/10.1364/OE.11.002982

[5] Wang, Y., Xu, Ch.-Q. & Po, H. Thermal effects in kilowatt fiber lasers. *IEEE Photonics Technol. Lett.* **16**, 63–65 (2004). https://doi.org/10.1109/LPT.2003.818913

[6] Zintzen, B., Langer, T., Geiger, J., Hoffmann, D. & Loosen, P. Heat transport in solid and air-clad fibers for high-power fiber lasers. *Opt. Express* **15**, 16787–16793 (2007). https://doi.org/10.1364/OE.15.016787

[7] Lapointe, M.-A., Chatigny, S., Piché, M., Cain-Skaff, M. & Maran, J.-N. Thermal effects in high-power CW fiber lasers. in *Fiber Lasers VI: Technology, Systems, and Applications*, *Proc. SPIE* **7195**, 430–440 (2009). https://doi.org/10.1117/12.809021

[8] Liu, T., Yang, Z. M. & Xu, S. H. Analytical investigation on transient thermal effects in pulse end-pumped short-length fiber laser. *Opt. Express* **17**, 12875–12890 (2009). https://doi.org/10.1364/OE.17.012875

[9] Sabaeian, M., Nadgaran, H., Sario, M. D., Mescia, L. & Prudenzano, F. Thermal effects on double clad octagonal Yb:glass fiber laser. *Opt. Mater.* **31**, 1300–1305 (2009). https://doi.org/10.1016/j.optmat.2008.10.034

[10] Ashoori, V. & Malakzadeh, A. Explicit exact three-dimensional analytical temperature distribution in passively and actively cooled high-power fibre lasers. *J. Phys. D.* **44**, 355103 (2011). https://doi.org/10.1088/0022-3727/44/35/355103

[11] Fan, Y. *et al*. Thermal effects in kilowatt all-fiber MOPA. *Opt. Express* **19**, 15162–15172 (2011). https://doi.org/10.1364/OE.19.015162

[12] Fan, Y. *et al*. Efficient heat transfer in high-power fiber lasers. *Chin. Opt. Lett.* **10**, 111401–111401 (2012). http://col.osa.org/abstract.cfm?URI=col-10-11-111401

[13] Huang, C. *et al*. A versatile model for temperature-dependent effects in Tm-doped silica fiber lasers. *J. Light. Technol.* **32**, 421–428 (2014). https://doi.org/10.1109/JLT.2013.2283294

[14] Mohammed, Z., Saghafifar, H. & Soltanolkotabi, M. An approximate analytical model for temperature and power distribution in high-power Yb-doped double-clad fiber lasers. *Laser Phys.* **24**, 115107 (2014). https://doi.org/10.1088/1054-660X/24/11/115107

[15] Yang, J., Wang, Y., Tang, Y. & Xu, J. Influences of pump transitions on thermal effects of multi-kilowatt thulium-doped fiber lasers. arXiv preprint arXiv:1503.07256 (2015). https://arxiv.org/abs/1503.07256

[16] Daniel, J. M. O., Simakov, N., Hemming, A., Clarkson, W. A. & Haub, J. Metal clad active fibres for power scaling and thermal management at kW power levels. *Opt. Express* **24**, 18592–18606 (2016). https://doi.org/10.1364/OE.24.018592

[17] Karimi, M. Theoretical study of the thermal distribution in Yb-doped double-clad fiber laser by considering different heat sources. *Prog. Electromagn. Res. C* **88**, 59–76 (2018). https://doi.org/10.2528/PIERC18081505

[18] Lv, Y., Zheng, H. & Liu, S. Analytical thermal resistance model for high power double-clad fiber on rectangular plate with convective cooling at upper and lower surfaces. *Opt. Commun.* **419**, 141–149 (2018). https://doi.org/10.1016/j.optcom.2018.03.001

[19] Mafi, A. Temperature distribution inside a double-cladding optical fiber laser or amplifier. *J. Opt. Soc. Am. B* **37**, 1821–1828 (2020). https://doi.org/10.1364/JOSAB.390935

[20] Peterka, P. *et al*. Thulium-doped silica-based optical fibers for cladding-pumped fiber amplifiers, *Opt. Mater.* **30**, 174–176 (2007). https://doi.org/10.1016/j.optmat.2006.11.039

[21] Peterka, P., Faure, B., Blanc, W., Karásek, M. & Dussardier, B. Theoretical modelling of S-band thulium-doped silica fibre amplifiers. *Opt. Quantum Electron.* **36**, 201–212 (2004). https://doi.org/10.1023/B:OQEL.0000015640.82309.7d

[22] Koška, P., Peterka, P. & Doya, V. Numerical modelling of pump absorption in coiled and twisted double-clad fibers. *IEEE J. Sel. Topics Quantum Electron.* **22**, 55–62 (2016). https://doi.org/10.1109/JSTQE.2015.2490100

[23] Darwich, D. *et al*., 140 µm single-polarization passive fully aperiodic large-pitch fibers operating near 2 µm. *Appl. Opt.* **56**, 9221–9224 (2017). https://doi.org/10.1364/AO.56.009221

[24] Franczyk, M., Stępień, R., Filipkowski, A., Pysz, D. & Buczyński, R. Nanostructured core active fiber based on ytterbium doped phosphate glass. *IEEE J. Light. Technol.* **37**, 5885–5891 (2019). https://doi.org/10.1109/jlt.2019.2941664

[25] Michalska, M., Brojek, W., Rybak, Z., Sznelewski, P., Mamajek, M. & Świderski, J. Highly stable, efficient Tm-doped fiber laser—a potential scalpel for low invasive surgery. *Laser Phys. Lett.* **13**, 115101 (2016). https://doi.org/10.1088/1612-2011/13/11/115101

[26] Todorov, F. *et al*. Active optical fibers and components for fiber lasers emitting in the 2-µm spectral range. *Materials* **13**, 5177 (2020). https://doi.org/10.3390/ma13225177

[27] Engineering ToolBox. Air – thermal conductivity. (2009). https://www.engineeringtoolbox.com/air-properties-viscosity-conductivity-heat-capacity-d_1509.html

[28] Schreiber, T., Eberhardt, R., Limpert, J. & Tunnermann, A. High-power fiber lasers and amplifiers: fundamentals and enabling technologies to enter the upper limits. in *Fiber lasers* 7–61 (ed. Okhotnikov, O. G.) (Wiley-VCH, 2012). https://doi.org/10.1002/9783527648641.ch2

[29] Limpert, J. *et al*. High-power rod-type photonic crystal fiber laser, *Opt. Express* **13**, 1055–1058 (2005). https://doi.org/10.1364/OPEX.13.001055

[30] Limpert, J. *et al*. Yb-doped large-pitch fibres: effective single-mode operation based on higher-order mode delocalisation. *Light Sci. Appl.* **1**, e8 (2012). https://doi.org/10.1038/lsa.2012.8